ISPRS Journal of Photogrammetry and Remote Sensing ▮ (▮▮▮▮) ▮▮▮–▮▮▮

Contents lists available at ScienceDirect

ISPRS Journal of Photogrammetry and Remote Sensing

journal homepage: www.elsevier.com/locate/isprsjprs

Expanding global mapping of the foliage clumping index with multi-angular POLDER three measurements: Evaluation and topographic compensation

Jan Pisek [a,b,*], Jing M. Chen [a], Roselyne Lacaze [c], Oliver Sonnentag [d], Krista Alikas [b]

[a] University of Toronto, Department of Geography and Program in Planning, Sidney Smith Hall, 100 St. George Street, Room 5047, Toronto, ON, Canada M5S 3G3

[b] Tartu Observatory, 61602 Tõravere, Estonia

[c] CESBIO, Toulouse Cedex, France

[d] University of California Berkeley, Berkeley, USA

ARTICLE INFO

Article history:
Received 15 August 2009
Received in revised form
7 February 2010
Accepted 10 March 2010
Available online xxxx

Keywords:
Multi-angle remote sensing
Vegetation clumping index
POLDER
BRDF

ABSTRACT

The clumping index measures the spatial aggregation (clumped, random and regular) of foliage elements. The global mapping of the clumping index with a limited eight-month multi-angular POLDER 1 dataset is expanded by integrating new, complete year-round observations from POLDER 3. We show that terrain-induced shadows can enhance bi-directional reflectance distribution function variation and negatively bias the clumping index (i.e. indicating more vegetation clumping) in rugged terrain. Using a global high-resolution digital elevation model, a topographic compensation function is devised to correct for this terrain effect. The clumping index reductions can reach up to 30% from the topographically non-compensated values, depending on terrain complexity and land cover type. The new global clumping index map is compared with an assembled set of field measurements from 32 different sites, covering four continents and diverse biomes.

1. Introduction

The clumping index quantifies the level of foliage grouping within distinct canopy structures, such as tree crowns, shrubs, and row crops, relative to a random distribution (Nilson, 1971; Chen et al., 2005; Weiss et al., 2004). The clumping index is useful in ecological and meteorological models because it provides new structural information to the effective leaf area index L_e (Chen and Black, 1991), where L_e is defined as one half of the total area of light intercepting leaves per unit horizontal ground surface area, assuming that the foliage spatial distribution is random (Black et al., 1991). Clumping, through a better separation of sunlit and shaded leaves, has profound effects on the radiation regime of a plant canopy and photosynthesis (Baldocchi and Harley, 1995; Mõttus et al., 2006). As the clumping index can vary considerably for a land cover type, it is highly desirable to map the spatial distribution of this index using remote sensing data (Chen et al., 2003). The clumping index (Ω) larger than unity implies that the foliage is regularly distributed; $\Omega = 1$ for a random distribution and in the case of foliage more clumped than random, $\Omega < 1$ (Chen et al., 2005).

Previous studies have shown that the clumping index is related to the shape of bidirectional reflectance distribution function (BRDF) (Lacaze et al., 2002; Chen et al., 2003). Quantitatively, the clumping index can be associated with an angular index formulated using the hotspot (where the sun and view angles coincide) and the darkspot (where the reflectance is at its minimum) values from the BRDF curve along the principal plane (Leblanc et al., 2005). The normalized difference between hotspot and darkspot (NDHD) has been found to be linearly related to the clumping index (Chen et al., 2003; Simic et al., 2010). It is defined as

$$\mathrm{NDHD} = \frac{\rho_h - \rho_d}{\rho_h + \rho_d} \quad (1)$$

where ρ_h and ρ_d are the reflectance at the hotspot and darkspot, respectively. The clumping index information is included in the darkspot reflectance, whereas the hotspot can be seen as the normalizing factor when used in NDHD (Chen et al., 2003). The relationship between clumping index and darkspot exists mostly because clumped canopies cast dark shadows and decrease the darkspot reflectance (Leblanc et al., 2005). The relationship was previously used to derive a first-ever global clumping index map using multi-angular POLDER 1 satellite data from ADEOS-1 (Chen et al., 2005). The original POLDER 1 global clumping index map had several limitations that are addressed by this study: limited spatial coverage, topographic effects, and a lack of evaluation with field measurements.

* Corresponding author at: University of Toronto, Department of Geography and Program in Planning, Sidney Smith Hall, 100 St. George Street, Room 5047, Toronto, ON, Canada M5S 3G3. Tel.: +1 416 978 5070.

E-mail address: jan.pisek@utoronto.ca (J. Pisek).

0924-2716/$ – see front matter © 2010 International Society for Photogrammetry and Remote Sensing, Inc. (ISPRS). Published by Elsevier B.V. All rights reserved.
doi:10.1016/j.isprsjprs.2010.03.002

2. Expanding the global clumping index map with POLDER 3

The POLDER radiometer is designed to measure directional and polarized reflectances of the Earth's surface–atmosphere system (Deschamps et al., 1994). The instrument concept consists of a rotating wheel equipped with and without polarized filters, a CCD matrix array detector, and a wide field of view lens (114°) that gives a swath about 2400 km, which allows the same ground area to be viewed during successive orbital passes. During a single satellite overpass, a surface target is scanned up to 14 (POLDER 1) or 16 times (POLDER 3) under different viewing angles. The view illumination directional configuration changes every day as the orbit shifts. Therefore, after a few days, assuming clear atmospheric conditions, the measurements provide a sample of the BRDF within the sensor field of view. POLDER is best used at the global scale because of its ~6 km nadir resolution and high angular resolution. For the expansion of the original global clumping index map, we used data from POLDER 3 onboard PARASOL microsatellite (Lier and Bach, 2008). Available POLDER 3 data, provided by MEDIAS-France/POSTEL Service Centre, cover the whole year 2005.

The clumping index was calculated using the NIR band and relationship between NDHD and Ω, i.e.,

$$\Omega = a + b\,\mathrm{NDHD} \tag{2}$$

where a and b are coefficients determined by the linear regression, based on a set of model simulations made with 4-Scale model (assuming a flat terrain) in Chen et al. (2005). The coefficients are the same as for POLDER 1 data and vary with solar zenith angle (SZA) and vegetation type (see Table 2 in Chen et al., 2005). Pinty et al. (2002) assert that the wavelength should be chosen to maximize the reflectance/absorption contrasts between vertically clumped elements and the background, i.e. the red band should be more appropriate due to weaker multiple scattering (Pinty et al., 2009). However, a stronger relationship between NDHD and Ω in the NIR band was observed previously both with 4-Scale modeled (Chen et al., 2005) and CASI airborne data (Simic et al., 2010). This, coupled with the greater accuracy limitations in the atmospheric correction in the red band for satellite data, led to the choice of the NIR band for clumping index retrieval here.

The land cover information was obtained from Global Land Cover 2000 (GLC2000) database (Bartholomé and Belward, 2005). The clumping index was first calculated on a monthly basis with available data from POLDER 1 and POLDER 3 separately. For each pixel, the monthly maps covering the summer half-year season for the respective hemisphere were then averaged to obtain the mean clumping index values for the main vegetation growing period. POLDER 3 data improved the global coverage with valid Ω retrievals over vegetated areas by 7.5% up to 95%, mainly over North America and northern Asia. However, even more important was the possibility of finally obtaining Ω for the Northern Hemisphere during the periods of peak vegetation growth, since POLDER 1 was active only from November 1996 to June 1997. The remaining gaps are mainly in the tropic regions due to persistent cloud cover.

3. Reduction of topographic effects in the global clumping index map

Topography might have a severe impact on NDHD due to shadowing, adjacent hill illumination, sky occlusion, and slope orientation with respect to the BRDF of the land cover type (Schaaf et al., 1994). The reliable reconstruction of the BRDF to obtain non-biased hotspot and darkspot values in rugged terrain is more challenging than it is from a similarly vegetated flat region as the BRDF is no longer symmetrical on the principal plane (Schaaf et al., 1994). Direct correction of the BRDF would be impractical here due to the global spatial extent, frequency, and the number of different angular configurations during POLDER observations. Thus, a simple and robust correction for influences of rugged terrain is required.

A global digital elevation model (DEM) GTOPO30 with 30-arc seconds (~1 km) grid spacing from US Geological Survey's EROS Data Center in Sioux Falls, South Dakota,[1] was used to examine effects of topographic variation on the NDHD and Ω. Average elevation, standard deviation and slope were calculated within each POLDER pixel (~6 km resolution). A negative correlation (i.e. more clumped vegetation with increasing values of terrain parameters) was observed across all vegetation land cover types. The strongest relationship was obtained for standard deviation of elevation within POLDER pixels (Fig. 1(a)). High elevation variation induces terrain shadows that can also increase the BRDF variation (Sandmeier and Itten, 1997). Additionally, canopy mutual shadowing also increases with terrain complexity (Soenen et al., 2005). Since the information about the vegetation clumping is mainly included in the darkspot (Chen et al., 2005), shadows cast from neighboring terrain features and increased self-shadowing result in negatively biased values of Ω. The observed change in Ω is not linear with the variation of elevation (Fig. 1(a)). The change course is also similar to the modeling work of Kane et al. (2008), where the nonlinearity was related to the changing role of sunlit and shaded areas of canopy on the total reflectance.

Topographically uncorrected Ω values from Eq. (2) are formed by the contributions from (a) land cover type-independent, terrain-induced shadows, and (b) the actual structural properties of foliage (e.g. leaf area distribution within crowns, organization of needles into shoots and whorls), which at the coarse ~6 km resolution of POLDER instrument shall not be closely dependent on topographic complexity. Topographically corrected Ω from POLDER data is not expected to show any trend with increasing standard deviation of elevation (σ). The effect of topography, demonstrated through the increasing difference between Ω at $\sigma_{i=0}$ (flat terrain) and Ω at $\sigma_{i+1,i+2,\ldots,i+y}$ (increasing topographic variation) in Fig. 1(a), was removed in four steps. First, all valid clumping index retrievals from the compiled global clumping index map in Section 2 were binned into 50-m interval classes by the value of σ for given pixel, and the mean clumping index value was retrieved for every class interval (Fig. 1(a)). Second, a polynomial function was fitted to the observed decrease in Ω with σ by the following polynomial function ($R^2 = 0.99$) (Fig. 1(a)):

$$\Omega_T = -0.0000001\sigma^3 + 0.000117\sigma^2 - 0.0605\sigma + 70.1 \tag{3}$$

where Ω_T values describe primarily the observed across-biome, terrain shadow-induced decreasing trend in Ω with increasing topographic complexity, represented by σ. Since this polynomial function is fitted to the mean values of both forest and non-forest pixels at each σ interval, the foliage structure effect in Ω_T values is suppressed. The area fractions of biome types in each σ range might have influenced this regression, but as the critical forest fraction varies in a limited range (0.42–0.66) (Fig. 1(a)), this influence would be less than 0.05 in the final Ω value. Next, for each POLDER pixel the difference δ between original Ω and Ω_T was calculated. Finally, δ was added to the intercept from Eq. (3). In this way, the across-biome difference in the topographical effect was removed, while the role of foliage structure was retained. The topographically corrected global average clumping index still decreases with σ; however, now this decrease is related to the increased share of forest (i.e. more clumped) areas in the rugged terrain (Fig. 1(a)). The new forest-only clumping index values oscillate around $\Omega = 0.66$ and become independent of terrain complexity. Despite rather smaller area of more topographically

[1] http://edc2.usgs.gov/geodata/index.php.

Please cite this article in press as: Pisek, J., et al., Expanding global mapping of the foliage clumping index with multi-angular POLDER three measurements: Evaluation and topographic compensation. ISPRS Journal of Photogrammetry and Remote Sensing (2010), doi:10.1016/j.isprsjprs.2010.03.002

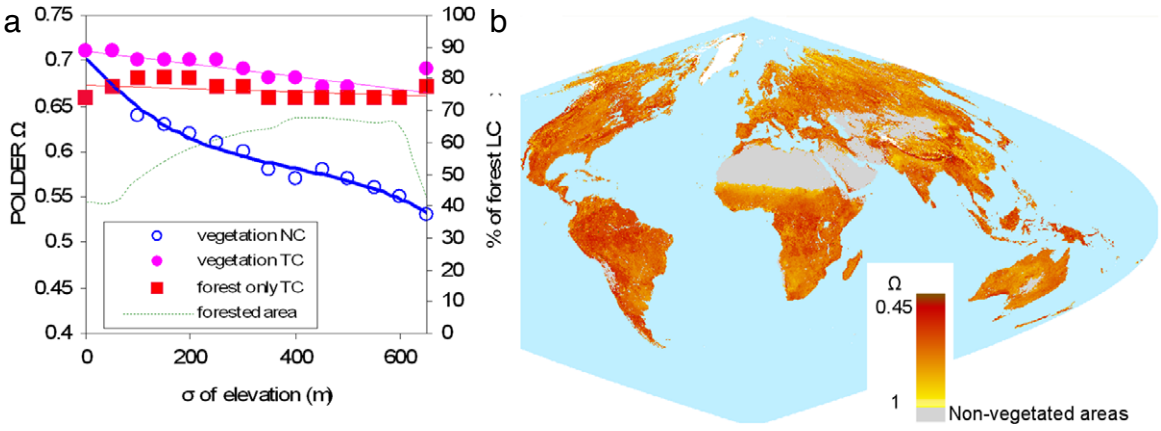

Fig. 1. (a) Global mean clumping index (Ω) values over vegetated areas against standard deviation (σ) of elevation within POLDER pixels. The polynomial function (Eq. (3)) is fitted to the topographically uncorrected Ω values (blue empty circles). The decreasing trend in the topographically corrected Ω values (filled circles in violet) is caused by increasing share of forested area in rugged terrain. Topographically corrected Ω values for forest-only areas oscillate around a constant value (red line; filled squares). In the legend, NC—Ω topographically not compensated, TC—Ω topographically compensated. (b) The new, topographically corrected global vegetation clumping index map derived from POLDER 1 and POLDER 3 data using the normalized difference between interpolated hotspot and darkspot NIR reflectance and applied to vegetated land cover. (For interpretation of the references to colour in this figure legend, the reader is referred to the web version of this article.)

Table 1
Average statistics calculated with the topographically corrected clumping index values over vegetated areas.

Class	Class names	Mean	Stan. dev.
1	Tree cover, broadleaf, evergreen	0.64	0.11
2	Tree cover, broadleaf, deciduous, closed	0.69	0.08
3	Tree cover, broadleaf, deciduous, open	0.72	0.05
4	Tree cover, needleleaf, evergreen	0.63	0.12
5	Tree cover, needleleaf, deciduous	0.78	0.07
6	Tree cover, mixed leaf type	0.72	0.11
7	Tree cover, regularly flooded, fresh water	0.67	0.15
8	Tree cover, regularly flooded, saline water	0.78	0.17
9	Mosaic: Tree cover/other natural vegetation	0.70	0.05
10	Tree cover, burnt	0.78	0.15
11	Shrub cover, closed-open, evergreen	0.77	0.17
12	Shrub cover, closed-open, deciduous	0.74	0.09
13	Herbaceous cover, closed-open	0.77	0.12
14	Sparse herbaceous or sparse shrub cover	0.78	0.16
15	Reg. flooded shrub and/or herbaceous cover	0.80	0.14
16	Cultivated and managed areas	0.78	0.11
17	Mosaic: cropland/tree cover/natural veg	0.77	0.12
18	Mosaic: cropland/shrub and/or grass cover	0.76	0.05

complex terrain (e.g. only around 15% of all ~6 km resolution POLDER pixels with vegetation have a standard deviation of elevation σ greater than 100 m; their fraction drops to 5% by σ of 250 m), the clumping index reductions can reach up to 30% in the new topographically corrected global clumping index map, depending on terrain complexity and land cover type (Fig. 1(b)). Average statistics for the topographically corrected clumping index values still retain the relative differences between the various land cover types (Table 1). Finally, gaps in the global coverage by POLDER observations (5% of vegetated areas, mainly in the tropics due to persistent cloud cover) are filled with mean clumping index values calculated from the successful retrievals over the same biomes (Table 1) for the dominant land cover types from the GLC2000 map to obtain the updated global clumping index map (Fig. 1(b)).

4. Evaluation of the new global clumping index map

At the scale of the POLDER data (~6 km), it is very difficult to evaluate the clumping index map and no previous attempts are reported in the literature. Larger ground truth plots are necessary for clumping index evaluation because of the POLDER resolution. The considered sites had a dominant land cover type at ~6 km resolution (i.e. a single GLC2000 land cover type containing over 65% of area within the corresponding POLDER pixel) that was coincident with the land cover type sampled in the field. Another difficulty for direct comparison stems from the fact that the POLDER-derived clumping index quantifies the total effect of canopy structures at all levels on radiation interception and photosynthesis by the canopy (Lacaze et al., 2002). The total clumping index Ω can be separated into two components, namely clumping at a scale larger and smaller than the shoot, which are measured separately in the field and in the lab:

$$\Omega = \frac{\Omega_E}{\gamma_E} \tag{4}$$

where Ω_E is the clumping of foliage elements, leaves for broadleaf species and shoots for needleleaf species; and γ_E is the needle-to-shoot area ratio, which accounts for clumping of needles into shoots; for broadleaves $\gamma_E = 1$ (Chen et al., 1997). Further, different methods and equations exist for obtaining Ω_E from field measurements, although most of them are highly correlated (for a brief list and comparison see Gonsamo and Pellikka, 2009). Ω_E has been also shown to be dependent on the solar zenith angle (Kucharik et al., 1999; Ryu et al., 2010), but the angular dependence follows patterns that allow it to be estimated from only one angular measurement of clumping with instrument such as Tracing Radiation and Architecture of Canopies (TRAC) (Chen, 1996). For the preliminary evaluation we compiled a database of clumping index field measurements with TRAC from 32 different sites, covering four continents and diverse biomes (Table 2). However, it must be acknowledged that the spatial and biome coverage of the available measurements is still limited and can be considered rather biased towards temperate/boreal regions (62% of the sites are in Canada; 82% of the sites are over the 40 °N parallel; only 31% of the sites are non-coniferous).

The field data should be optimally integrated with high-resolution imagery to allow a real product validation (Morisette et al., 2006). Unfortunately, with only one exception of a limited-extent high resolution map of clumping index (<1 km^2) by Simic et al. (2010), no such maps are currently available, allowing only a limited evaluation. In the absence of high-resolution maps of the clumping index, the Ω_E measurements with TRAC are the most suitable for comparison with the retrievals from POLDER data since the instrument is walked along transects that are in the range of tens or hundreds of meters. While Ω_E estimates can also be obtained from hemispherical photography (HP) (see e.g. Gonsamo et al., in press; Leblanc et al., 2005; Walter et al., 2003), the length

Please cite this article in press as: Pisek, J., et al., Expanding global mapping of the foliage clumping index with multi-angular POLDER three measurements: Evaluation and topographic compensation. ISPRS Journal of Photogrammetry and Remote Sensing (2010), doi:10.1016/j.isprsjprs.2010.03.002

Table 2
Characteristics and results from the validation sites and POLDER retrievals.

ID	Site	Location	Lat	Lon	Overstory	Dates	Transect lengths (m)	γ_E	Field Ω_E	Method	Field Ω	POLDER Ω	Ref.
1	Mongu	Zambia	15.44 °S	23.25 °E	W	2000/3	3 × 750	1	0.76	CC	0.76	0.77	1
2	Pandametanga	Botswana	18.66 °S	25.5 °E	OW	2000/3	3 × 750	1	0.69	CC	0.69	0.71	1
3	Maun	Botswana	19.92 °S	23.59 °E	MW	2000/3	3 × 750	1	0.76	CC	0.76	0.77	1
4	Okwa River	Botswana	22.41 °S	21.71 °E	Osh	2000/3	3 × 750	1	0.57	CC	0.57	0.58	1
5	Tshane	Botswana	24.16 °S	21.89 °E	Osa	2000/3	3 × 750	1	0.72	CC	0.72	0.8	1
6	Heihe	China	38.02 °N	101.25 °E	AM	2002/7	5 × 20	1	0.95	CC_N	0.95	0.89	2
7	Tonzi	USA	38.43 °N	120.97 °W	BO, CFP	2008/9	4 × 90	1	0.82	CC_N	0.82	0.82	3
8	NOJP	Canada	55.928 °N	98.624 °W	OJP	1994/S	210	1.42	0.82	CC	0.58	0.59	4
9	SOJP	Canada	53.916 °N	104.692 °W	OJP	1994/S	200	1.51	0.71	CC	0.47	0.64	4
10	NYJP	Canada	55.905 °N	98.288 °W	YJP	1994/S	340	1.45	0.95	CC	0.66	0.63	4
11	SYJP	Canada	53.877 °N	104.697 °W	YJP	1994/S	300	1.37	0.72	CC	0.53	0.61	4
12	NOBS	Canada	55.88 °N	98.484 °W	OBS	1994/S	300	1.45	0.71	CC	0.49	0.71	4
13	SOBS	Canada	53.987 °N	105.122 °W	OBS	1994/S	300	1.45	0.7	CC	0.48	0.58	4
14a	Petawawa_a	Canada	46 °N	77.45 °W	RP	1993/9	2 × 60	2.08	0.91	CC	0.44	↓	5
14b	Petawawa_b	Canada	46 °N	77.45 °W	JP	1993/9	2 × 50	1.3	0.88	CC	0.68	↓	5
14	Petawawa										0.56	0.64	
15	Metolius	USA	44.30 °N	121.37 °W	PP	1997/9	100	1.25	0.81	CC	0.65	0.71	6
16a	Kananaskis_a	Canada	51.02 °N	115.06 °W	LpP	1999/S	10 × 10	2.08	0.88	CC_N	0.42	↓	7
16b	Kananaskis_b	Canada	51.02 °N	115.06 °W	WS	1999/S	10 × 10	1.27	0.89	CC_N	0.70	↓	7
16c	Kananaskis_c	Canada	51.02 °N	115.06 °W	A, BP	1999/S	10 × 10	1	0.87	CC_N	0.87	↓	7
16	Kananaskis										0.66	0.63	
17	F77	Canada	54.485 °N	105.817 °W	JP	2003–2005/S	100	1.4	0.99	CC_N	0.71	0.71	8
18	F98	Canada	53.917 °N	106.078 °W	JP	2003-2005/S	100	1.4	0.97	CC_N	0.69	0.61	8
19	SOJP	Canada	53.916 °N	104.69 °W	JP	2003–2005/S	200, 60	1.42	0.85	CC_N	0.60	0.64	8
20	HJP75	Canada	53.875 °N	104.045 °W	JP	2003–2005/S	150, 150	1.44	0.93	CC_N	0.65	0.65	8
21	HJP94	Canada	53.908 °N	104.69 °W	JP	2003–2005/S	100	1.44	0.83	CC_N	0.58	0.64	8
22	SOBS	Canada	53.987 °N	105.117 °W	OBS	2003–2005/S	100, 60	1.36	0.9	CC_N	0.66	0.58	8
23a	Mer Bleue	Canada	45.4 °N	75.5 °W	BS	2005/8	100	1.36	0.87	CC_N	0.64	↓	9
23b	Mer Bleue	Canada	45.4 °N	75.5 °W	T	2005/8	100	1.42	0.87	CC_N	0.61	↓	9
23	Mer Bleue										0.63	0.62	
24	Sudbury	Canada	47.16 °N	81.75 °W	BS, JP	2007/6	5 × 40	1.35	0.82	CC_N	0.61	0.59	10
25	Takayama	Japan	36.1462 °N	137.4231 °E	JO	2006/S	2 × 100	1	0.93	CC_N	0.93	0.83	11
26	Appomattox	USA	37.219 °N	78.879 °W	LbP	2002/8	5 × 100	1.21	0.89	CC_N	0.74	0.76	12
27	SETRES	USA	34.90 °N	79.49 °W	LbP	2003/8	3 × 100	1.21	0.899	CC_N	0.74	0.77	13
28	Hertford	USA	36.383 °N	77.001 °W	LbP	2003/8	5 × 100	1.21	0.94	CC_N	0.78	0.74	14
29	Black Hills	USA	43.8 °N	103.88 °W	PP	2002–2003/7, 8	6 × 25	1.25	0.83	CC_N	0.66	0.67	15
30	Yatir	Israel	31.21 °N	35.02 °E	AP	2004/4	200	1.21	0.84	CC_N	0.69	0.73	16
31a	Jarvselja_a	Estonia	58.25 °N	27.46 °E	B	2008/7	60, 90	1	0.93	CC_N	0.93	↓	17
31b	Jarvselja_b	Estonia	58.25 °N	27.46 °E	NS	2008/7	60, 90	1.56	0.84	CC_N	0.54	↓	17
31c	Jarvselja_c	Estonia	58.25 °N	27.46 °E	SP	2008/7	60, 90	1.75	0.85	CC_N	0.49	↓	17
31	Jarvselja										0.65	0.72	
32a	Bily Kriz_a	Czech Rep.	49.30 °N	18.32 °E	NS_Y	2006/9	7 × 70	1.526	0.89	CC_N	0.58	↓	18
32b	Bily Kriz_b	Czech Rep.	49.30 °N	18.32 °E	NS_O	2006/9	7 × 70	1.422	0.67	CC_N	0.47	↓	18
32	Bily Kriz										0.53	0.61	

"Lat", "Lon", "Ref" stand for "latitude", "longitude" and "reference", respectively. In the column "Site" the number indicates the ID of the site. In the column "Overstory" W—woodland, OW—open woodland, MW—mopane woodland, Osh—open shrubland, Osa—open savanna, AM—alpine meadow, BO—blue oak, CFP—California foothill pine, OJP—old jack pine, YJP—young jack pine, OBS—old black spruce, RP—red pine, JP—jack pine, PP—ponderosa pine, LpP—lodgepole pine, WS—white spruce, A—aspen, BP—balsam poplar, BS—black spruce, T—tamarack,, JO—Japanese oak, LbP—Loblolly pine, AP—alepo pine, B—birch, NS—Norway spruce, SP—scots pine, NS_0—Norway spruce old, NS_Y—Norway spruce young. In the column "Dates", S stands for summer. In the column "Method" CC stands for the Chen and Cihlar (1995) method of calculating Ω_E, CC_N stands for the normalized CC method by Leblanc (2002). The column "Ref." indicates the associated references for the validation sites. The numbers refer to 1: (Privette et al., 2004), 2: (Lu et al., 2005), 3: (Ryu et al., 2010) 4: Ω_E from (Chen et al., 1997), γ_E from (Chen, 1996), 5: (Chen and Cihlar, 1995), 6: (Law et al., 2001), 7: (Hall et al., 2003), 8: (Chen et al., 2006), 9: (Sonnentag et al., 2007), 10: (Pisek et al., 2010), 11: (Nasahara et al., 2008), 12: (Iiames et al., 2006), 13: (Iiames et al., 2008), 14: (Iiames et al., 2004), 15: (Pocewicz et al., 2007), 16: (Sprintsin et al., 2007), 17: (Pisek and Alikas, 2008), 18: (Homolová et al., 2007). All the measurements were taken within the solar zenith range of 30°–60°.

of suitable angular rings (30°–60° view zenith angles; Leblanc and Chen, 2001) is substantially smaller compared to the length of TRAC-sampled transects (Table 2). As a result, clumping effects at landscape scales as observed by POLDER would be underestimated with HP retrievals. γ_E values were used as reported in the original papers (Table 2); otherwise default values for the tree species were used as suggested by Chen et al. (2006).

The agreement is very encouraging over woodland and savannas in Africa and USA, although the number of measurements is not very high (Fig. 2(a)). The disagreement between the field measurements for forest sites during the period of 1993–2001 (Fig. 2(b)) and 2002–2008 (Fig. 2(c)) is due to the missing normalization factor in the original derivation of Ω_E applied before 2002 (Leblanc, 2002). The effect of this correction can be confirmed by the relatively even distribution of the retrievals around 1:1 line for the post-2001 measurements (Fig. 2(c)), while non-normalized Ω_E values from 1993–2001 indicated rather higher clumping than retrievals from POLDER (Fig. 2(b)). The normalization effect is of concern in highly clumped stands (Law et al., 2001; Leblanc, 2002); the results over the presented savanna and woodlands should not be substantially affected, as the field Ω values with an exception of Okwa River site ($\Omega = 0.58$) indicate rather less clumped type of vegetation.

The mean absolute error (MAE) is 0.027 over savanna and woodland sites from Fig. 2(a), MAE = 0.046 for the forest sites measured from 2001–2008. However, these preliminary

Please cite this article in press as: Pisek, J., et al., Expanding global mapping of the foliage clumping index with multi-angular POLDER three measurements: Evaluation and topographic compensation. ISPRS Journal of Photogrammetry and Remote Sensing (2010), doi:10.1016/j.isprsjprs.2010.03.002

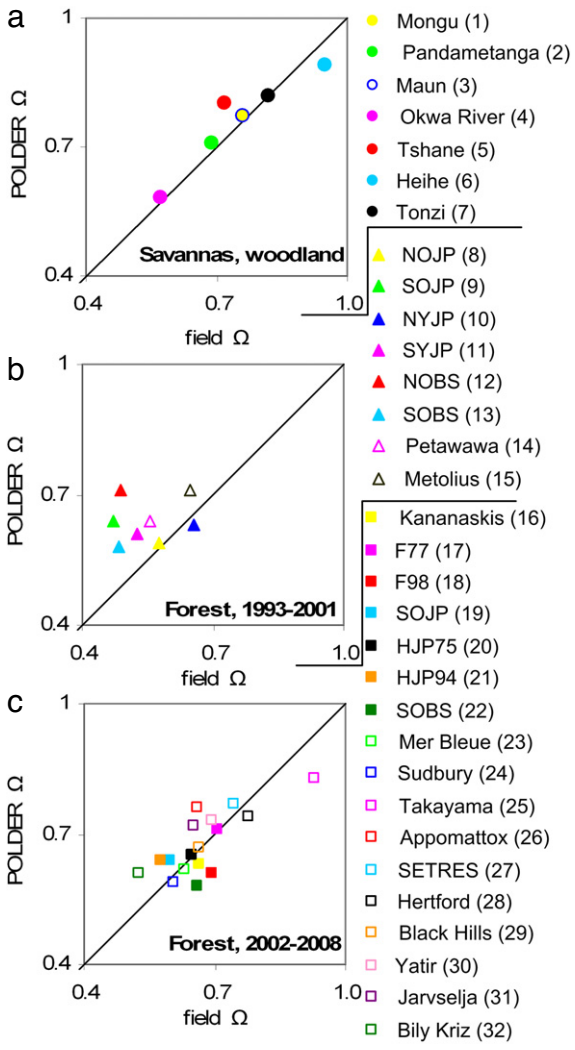

Fig. 2. Comparisons of POLDER Ω values with those from field measurements. Numbers in brackets correspond to site ID numbers in Table 2. (For interpretation of the references to colour in this figure legend, the reader is referred to the web version of this article.)

evaluation results should be still treated with caution due to the limited coverage of the compiled dataset especially over the non-boreal region, and the coarse resolution (~6 km) of the POLDER clumping map, particularly while considering its application to higher resolution/individual stand studies. For example, POLDER retrieval substantially underestimates the clumping index value (i.e. indicating more clumped foliage) for Pijnven site ($\Delta = -0.27$, not shown) with Scots Pine stand in Belgium (Jonckheere et al., 2005). The land cover in this area is very fragmented and the dominant land cover type from the GLC2000 dataset at POLDER resolution indicates cultivated and managed land, instead. The modeled results by Chen et al. (2005) also suggested that areas with less than 25% vegetation coverage or fragmented land cover should be treated with caution. Overall the new clumping index map achieves a good agreement with the homogeneous vegetation field site estimates. In light of the findings presented above, it is recommended to use the mean Ω values for land cover types from Table 1 in cases of heterogeneous land cover mosaic.

5. Conclusion

Multi-angle remote sensing techniques are currently under-utilized for ecological applications. Leaf area index and clumping index are two canopy structural parameters of comparable importance for plant growth and terrestrial carbon cycle modeling. In this context, it is expected that the findings and improvements of this study (a) will have a substantial impact on the use of the clumping index to improve the assessment of terrestrial productivity and carbon cycle before global clumping index maps at higher resolution are available, and (b) will encourage the highly needed acquisition of additional clumping index field measurements by TRAC or HP, especially for under-represented regions and biomes. The reconstruction of the BRDF in complex terrain shall also be considered in the future to obtain physically meaningful hot- and dark-spot values. The new global clumping index map presented in this study can be provided with quality flags upon request.

Acknowledgements

We are grateful to Centre National d'Etudes Spatiales for the provision of processed POLDER 1 and POLDER 3 data. This study is supported by the Natural Science and Engineering Council of Canada (Discovery Grant) and a student assistantship to the first author by the Centre for Global Change Science at the University of Toronto. The first author wishes to thank Tiit Nilson for discussions about the clumping index. Careful reading, constructive comments and suggestions by three anonymous reviewers greatly improved the initial version of the manuscript. Leslie Erin Quinn helped with English style corrections.

References

Baldocchi, D.D., Harley, P.C., 1995. Scaling carbon dioxide and water vapour exchange from leaf to canopy in a deciduous forest. II: Model testing and application. Plant, Cell and Environment 18 (10), 1157–1173.
Bartholomé, E., Belward, A.S., 2005. GLC2000: a new approach to global land cover mapping from Earth Observation data. International Journal of Remote Sensing 26 (9), 1959–1977.
Black, T.A., Chen, J.M., Lee, X., Sagar, R., 1991. Characteristics of shortwave and longwave irradiances under a Douglas-fir forest stand. Canadian Journal of Forest Research 21 (7), 1020–1028.
Chen, J.M., 1996. Optically-based methods for measuring seasonal variation of leaf area index in boreal conifer stands. Agricultural and Forest Meteorology 80 (2–4), 135–163.
Chen, J.M., Black, T.A., 1991. Measuring leaf area index of plant canopies with branch architecture. Agricultural and Forest Meteorology 57 (1), 1–12.
Chen, J.M., Cihlar, J., 1995. Plant canopy gap size analysis theory for improving optical measurements of leaf area index. Applied Optics 34 (27), 6211–6222.
Chen, J.M., Govind, A., Sonnentag, O., Zhang, Y., Barr, A., Amiro, B., 2006. Leaf area index measurements at Fluxnet Canada forest sites. Agricultural and Forest Meteorology 140 (1–4), 257–268. FCRN special issue.
Chen, J.M., Liu, J., Leblanc, S.G., Lacaze, R., Roujean, J.-L., 2003. Multi-angular optical remote sensing for assessing vegetation structure and carbon absorption. Remote Sensing of Environment 84 (4), 516–525.
Chen, J.M., Menges, C.H., Leblanc, S.G., 2005. Global mapping of foliage clumping index using multi-angular satellite data. Remote Sensing of Environment 97 (4), 447–457.
Chen, J.M., Rich, P.M., Gower, S.T., Norman, J.M., Plummer, S., 1997. Leaf area index of boreal forests: theory, techniques and measurements. Journal of Geophysical Research 102 (D24), 29429–29443.
Deschamps, P.Y., Breon, F.M., Leroy, M., Podaire, A., Bricaud, A., Buriez, J.C., Seze, G., 1994. The POLDER mission: instrument characteristics and scientific objectives. IEEE Transactions on Geosciences and Remote Sensing 32 (3), 598–615.
Gonsamo, A., Pellikka, P., 2009. The computation of foliage clumping index using hemispherical photography. Agricultural and Forest Meteorology 149 (10), 1781–1787.
Gonsamo, A., Walter, J.-M.N., Pellikka, P., 2010. Sampling gap fraction and size for estimating leaf area and clumping indices using hemispherical photography. Canadian Journal of Forest Research (in press).
Hall, R.J., Davidson, D.P., Peddle, D.R., 2003. Ground and remote estimation of leaf area index in Rocky Mountain forest stands, Kananaskis, Alberta. Canadian Journal of Remote Sensing 29 (3), 411–427.
Homolová, L., Malenovský, Z., Hanuš, J., Tomášková, I., Dvoráková, M., Pokorný, R., 2007. Comparison of different ground techniques to map leaf area index of Norway spruce forest canopy. In: Schaepman, M.E., Liang, S., Groot, N.E., Kneubühler, M. (Eds.), 10th Intl. Symposium on Physical Measurements and Spectral Signatures in Remote Sensing. The International Archives of the Photogrammetry. In: Remote Sensing and Spatial Information Sciences, vol. 36. pp. 499–504. Part 7/C50.

Iiames, J.S., Congalton, R.G., Pilant, A.N., Lewis, T.E., 2008. Validation of an integrated estimation of loblolly pine (Pinus taeda L.) leaf area index (LAI) using two indirect optical methods in the southeastern United States. Southern Journal of Applied Forestry 32 (3), 100–110.

Iiames, J.S., Pilant, A.N., Lewis, T.E., 2004. In-situ estimates of forest LAI for MODIS data validation. In: Lunetta, R.S., Lyon, J.G. (Eds.), Remote Sensing and GIS Accuracy Assessment. CRC, Boca Raton, FLA, pp. 41–58.

Iiames, J.S., Pilant, A.N., Lewis, T.E., Congalton, R.G., 2006. Assessment of MODIS LAI (v4) in Loblolly pine (P. taeda) forest site, Appomattox, Virgina. Global Vegetation Workshop, Missoula, MT, August 2006. http://www.ntsg.umt.edu/VEGMTG.2006/posters/Iiames_VegWorkshop_Missoula2006.ppt (accessed 20 February 2009).

Jonckheere, I., Muys, B., Coppin, P., 2005. Allometry and evaluation of in situ optical LAI determination in Scots pine: a case study in Belgium. Tree Physiology 25 (6), 723–732.

Kane, V., Gillespie, A., Mcgaughey, R., Lutz, J., Ceder, K., Franklin, J., 2008. Interpretation and topographic compensation of conifer canopy self-shadowing. Remote Sensing of Environment 112 (10), 3820–3832.

Kucharik, C.J., Norman, J.M., Gower, S.T., 1999. Characterization of radiation regimes in non-random forest canopies: theory, measurements, and simplified modeling approach. Tree Physiology 19 (11), 695–706.

Lacaze, R., Chen, J.M., Roujean, J.-L., Leblanc, S.G., 2002. Retrieval of vegetation index using hotspot signatures measured by the POLDER instrument. Remote Sensing of Environment 79 (1), 84–95.

Law, B.E., Van Tuyl, S., Cescatti, A., Baldocchi, D.D., 2001. Estimation of leaf area index in open-canopy ponderosa pine forests at different successional stages and management regimes in Oregon. Agricultural and Forest Meteorology 108 (1), 1–14.

Leblanc, S.G., 2002. Correction to the plant canopy gap size analysis theory used by the tracing radiation and architecture of canopies (TRAC) instrument. Applied Optics 41 (36), 7667–7670.

Leblanc, S.G., Chen, J.M., 2001. A practical scheme for correcting multiple scattering effects on optical LAI measurements. Agricultural and Forest Meteorology 110 (2), 125–139.

Leblanc, S.G., Chen, J.M., White, H.P., Latifovic, R., 2005. Canadawide foliage clumping index mapping from multi-angular POLDER measurements. Canadian Journal of Remote Sensing 31 (5), 364–376.

Lier, P., Bach, M., 2008. PARASOL a microsatellite in the A-Train for Earth atmospheric observations. Acta Astronautica 62 (2–3), 257–263.

Lu, L., Li, X., Huang, C.L., Ma, M.G., Che, T., Bogaert, J., Veroustraete, F., Dong, Q.H., Ceulemans, R., 2005. Investigating the relationship between ground-measured LAI and vegetation indices in an alpine meadow, north-west China. International Journal of Remote Sensing 26 (20), 4471–4484.

Morisette, J.T., Baret, F., Privette, J.L., Myneni, R.B., Nickeson, J.E., Garrigues, S., Shabanov, N.V., Weiss, M., Fernandes, R.A., Leblanc, S.G., Kalacska, M., Sanchez-Azofeifa, G.A., Chubey, M., Rivard, B., Stenberg, P., Rautiainen, M., Voipio, P., Manninen, T., Pilant, A.N., Lewis, T.E., Iiames, J.S., Colombo, R., Meroni, M., Busetto, L., Cohen, W.B., Turner, D.P., Warner, E.D., Petersen, G.W., Seufert, G., Cook, R., 2006. Validation of global moderate resolution LAI products: a framework proposed within the CEOS land product validation subgroup. IEEE Transactions in Geoscience and Remote Sensing 44 (7), 1804–1817.

Mõttus, M., Sulev, M., Lang, M., 2006. Estimation of crown volume for a geometric radiation model from detailed measurements of tree structure. Ecological Modelling 198 (3–4), 506–514.

Nasahara, K.N., Muraoka, H., Nagai, S., Mikami, H., 2008. Vertical integration of leaf area index in a Japanese deciduous broadleaved forest. Agricultural and Forest Meteorology 148 (6–7), 1136–1146.

Nilson, T., 1971. A theoretical analysis of the frequency of gaps in plant stands. Agricultural Meteorology 8 (1), 25–38.

Pinty, B., Lavergne, T., Widlowski, J.L., Gobron, N., Verstraete, M.M., 2009. On the need to observe vegetation canopies in the near-infrared to estimate visible light absorption. Remote Sensing of Environment 113 (1), 10–23.

Pinty, B., Widlowski, J.L., Gobron, N., Verstraete, M.M., Diner, D.J., 2002. Uniqueness of multi-angular measurements—Part 1: a subpixel surface heterogeneity indicator from MISR. IEEE Transactions on Geoscience and Remote Sensing 40 (7), 1560–1573.

Pisek, J., Alikas, K., 2008. Measuring beyond-shoot clumping at Jarvselja RAMI (Radiation transfer Modelling Intercomparison) test sites. Technical report, Tartu Observatory, Tõravere, Estonia, 2 p.

Pisek, J., Chen, J.M., Miller, J.R., Freemantle, J.R., Peltoniemi, J.I., Simic, A., 2010. Mapping forest background reflectance in a boreal region using multi-angle Compact Airborne Spectrographic Imager (CASI) data. IEEE Transactions on Geosciences and Remote Sensing 48 (1), 499–510.

Pocewicz, A., Vierling, L.A., Lentile, L.B., Smith, R., 2007. View angle effects on relationships between MISR vegetation indices and leaf area index in a recently burned ponderosa pine forest. Remote Sensing of Environment 107 (1–2), 322–333.

Privette, J.L., Tian, Y., Roberts, G., Scholes, R.J., Wang, Y., Caylor, K.K., Frost, P., Mukelabai, M., 2004. Vegetation structure characteristics and relationships of Kalahari woodlands and savannas. Global Change Biology 10 (3), 281–291.

Ryu, Y., Sonnentag, O., Nilson, T., Vargas, R., Kobayashi, H., Wenk, R., Baldocchi, D.D., 2010. How to quantify tree leaf area index in an open savanna ecosystem: a multi-instrument and multi-model approach. Agricultural and Forest Meteorology 150 (1), 63–76.

Sandmeier, S., Itten, K.I., 1997. A physically-based model to correct atmospheric and illumination effects in optical satellite data of rugged terrain. IEEE Transactions on Geosciences and Remote Sensing 35 (3), 708–717.

Schaaf, C.B., Li, X., Strahler, A.H., 1994. Topographic effects on bidirectional and hemispherical reflectances calculated with a geometric-optical canopy model. IEEE Transactions on Geosciences and Remote Sensing 32 (6), 1186–1193.

Simic, A., Chen, J.M., Freemantle, J., Miller, J.R., Pisek, J., 2010. Improving clumping and LAI algorithms based on multi-angle airborne imagery and ground measurements. IEEE Transactions on Geosciences and Remote Sensing 48 (4), 1742–1759.

Soenen, S.A., Peddle, D.R., Coburn, C.A., 2005. SCS+C: a modified sun-canopy sensor topographic correction in forested terrain. IEEE Transactions on Geosciences and Remote Sensing 43 (9), 2148–2159.

Sonnentag, O., Chen, J.M., Roberts, D.A., Talbot, J., Halligan, K.Q., Govind, A., 2007. Mapping tree and shrub leaf area indices in an ombrotrophic peatland through multiple endmember spectral unmixing. Remote Sensing of Environment 109 (3), 342–360.

Sprintsin, M., Karnieli, A., Berliner, P., Rotenberg, E., Yakir, D., Cohen, S., 2007. The effect of spatial resolution on the accuracy of leaf area index estimation for a forest planted in the desert transition zone. Remote Sensing of Environment 109 (4), 416–428.

Walter, J.-M.N., Fournier, R.A., Soudani, K., Meyer, E., 2003. Integrating clumping effects in forest canopy structure: an assessment through hemispherical photographs. Canadian Journal of Remote Sensing 29 (3), 388–410.

Weiss, M., Baret, F., Smith, G.J., Jonckheere, I., Coppin, P., 2004. Review of methods for in situ leaf area index (LAI) determination: Part II estimation of LAI, errors and sampling. Agricultural and Forest Meteorology 121 (1–2), 37–53.

Please cite this article in press as: Pisek, J., et al., Expanding global mapping of the foliage clumping index with multi-angular POLDER three measurements: Evaluation and topographic compensation. ISPRS Journal of Photogrammetry and Remote Sensing (2010), doi:10.1016/j.isprsjprs.2010.03.002